AGU ADVANCING EARTH AND SPACE SCIENCE

Geophysical Research Letters

RESEARCH LETTER
10.1029/2020GL092169

Key Points:

- Combined citizen scientist, all-sky image, and satellite data show a Strong Thermal Emission Velocity Enhancement (STEVE) occurring at 200–275 km
- Simultaneous observation of a STEVE occurring for a brief period of time close a much weaker SAR arc that lasts all night
- Satellite passes at the conjugate location show T_e and N_e perturbations associated with the STEVE and SAR arc in the northern hemisphere

Supporting Information:

Supporting Information may be found in the online version of this article.

Correspondence to:

C. Martinis,
martinis@bu.edu

Citation:

Martinis, C., Nishimura, Y., Wroten, J., Bhatt, A., Dyer, A., Baumgardner, J., & Gallardo-Lacourt, B. (2021). First simultaneous observation of STEVE and SAR arc combining data from citizen scientists, 630.0 nm all-sky images, and satellites. *Geophysical Research Letters*, *48*, e2020GL092169. https://doi.org/10.1029/2020GL092169

Received 23 DEC 2020
Accepted 19 MAR 2021

First Simultaneous Observation of STEVE and SAR Arc Combining Data From Citizen Scientists, 630.0 nm All-Sky Images, and Satellites

C. Martinis[1], Y. Nishimura[2], J. Wroten[1], A. Bhatt[3], A. Dyer[4], J. Baumgardner[1], and B. Gallardo-Lacourt[5,6]

[1]Center for Space Physics, Astronomy Department, Boston University, Boston, MA, USA, [2]Department of Electrical and Computer Engineering, Center for Space Physics, Boston University, Boston, MA, USA, [3]Center for Geospace Studies, SRI International, Menlo Park, CA, USA, [4]Citizen Scientist, Alberta, AB, Canada, [5]NASA Goddard Space Flight Center, Greenbelt, MD, USA, [6]Universities of Space Research Association, Columbia, MD, USA

Abstract On September 28, 2017 citizen scientist observations at Alberta, Canada (51°N, 113° W) detected aurora and a thin east-west purplish arc, known as strong thermal emission velocity enhancement (STEVE) that lasted less than 20 min. All-sky imagers at subauroral latitudes measured stable auroral red (SAR) arcs during the entire night. The imager at Bridger, MT (45.3°N, 108.9°W) also measured a STEVE. The overlapping geometry allowed to determine that the height of STEVE was 225–275 km. STEVE is brighter in the 630.0 nm images in the West and almost merges with the SAR arc in the East. A DMSP satellite pass in the southern hemisphere was at the conjugate location of the Bridger imager during the STEVE observation. When mapped into the northern hemisphere intense subauroral ion drift and subauroral polarization streams were detected associated with the two optical signatures measured in 630.0 nm.

Plain Language Summary STEVE (strong thermal emission velocity enhancement) and SAR (stable auroral red) arcs are optical phenomena occurring at sub-auroral latitudes. On September 28, 2017 images from a citizen scientist detected a bright STEVE. A nearby all-sky camera observing nighttime airglow with a 630.0 nm filter also measured it, allowing to determine the height of occurrence (~225–275 km). In addition, a weak SAR arc was also present. STEVE was brighter in the 630.0 nm images in the west and almost merged with the SAR arc in the east. A few minutes earlier a satellite was passing through the magnetically conjugate location of the all-sky imager, and data showed signatures coincident with STEVE and the SAR arc. Height emission was ~225–275 for STEVE and 300–350 km for the SAR arc.

1. Introduction

The subauroral region, located equatorward from typical auroral displays, has been extensively studied by investigating processes like subauroral polarization streams (SAPS), subauroral ion drifts (SAIDs), and stable auroral red (SAR) arcs. Recently a new optical phenomenon known as strong thermal emission velocity enhancement (STEVE) has brought renewed interest in this region (Gallardo-Lacourt, Liang, et al.,2018; MacDonald et al., 2018). A handful of papers have reported characteristics of STEVEs that seem to match those observed during SAIDs (Archer, Gallardo-Lacourt, et al., 2019; Nishimura et al., 2019). Spectrograph measurements show that the spectrum of STEVE contains two major contributing components: an overall enhancement of a continuous spectrum between 400 and 730 nm, with a peak at 630.0 nm (Gillies et al., 2019). Nevertheless there are still many issues that need to be understood. The initial observations made the assumption that STEVE was occurring at 130 km altitude, however a study using Citizen Scientist's photographs of a STEVE showed that it spanned altitudes from 130 to 270 km (Archer, St.-Maurice, et al., 2019). Altitudes of 150 and 250 km were also found using all-sky imagers (Liang et al., 2019).

Enhanced electron temperature and reduced ion density are typical signatures accompanying the observation of SAR arcs and STEVEs, as well as SAPS and SAIDs. These similarities make difficult to distinguish the optical signatures observed. In general, STEVEs are short lived, latitudinally thin, polychromatic (typically purple/mauve and white), and associated with very large westward flows (more than few km/s) (Archer, Gallardo-Lacourt et al., 2019), while SAR arcs are long lived, wide in latitude, monochromatic (630.0 nm),

Figure 1. Composite Panorama of aurora and strong thermal emission velocity enhancement (STEVE) observed on September 28, 2017 constructed from six individual frames showing green aurora to the North, reddish-purple aurora almost at zenith, and a mauve-white STEVE to the South. (Top): all-sky projection; (Bottom): rectangular projection.

and accompanied by weaker westward flows (<~1 km/s). STEVEs and SAR arcs can be distinguished if some of these parameters, like width, westward flow, or spectrum can be measured. A recent study by Liang et al. (2019) showed a high elevation STEVE that merged into a pre-existing SAR arc. They also showed that both arcs had similar brightness when observed in 630.0 nm. Harding et al. (2020) described a mechanism viable to produce the continuum spectrum characteristic of STEVE and discussed the differences with the 630.0 nm emission observed in SAR arcs.

The present study analyzes for the first time the simultaneous occurrence of a SAR arc and STEVE by using citizen scientist's photographs, an all-sky imager, and satellite data.

2. Observations

2.1. Citizen Scientist Observations

The data from citizen scientist auroral observers has provided critical information that helped to advance our knowledge of STEVEs. On September 28, 2017, auroral activity was observed in western Canada, most of northern and western North America, and it was registered by a citizen scientist in Alberta, Canada. Equatorward of the main auroral oval, STEVE appeared and lasted for about 20 min. After it faded away the main auroral display picked up again and moved overhead. Figure 1 shows a panorama in spherical (top) and rectangular (bottom) projections. The panorama was constructed from six individual frames, spaced every 60°, taken between 04:54 and 04:56 UT. Each exposure was 10 s at f/1.8 and ISO 2500. The spherical image is appropriate to compare with the image taken by the all-sky imager from Bridger. The zenith is at 51°N and 113°W and STEVE is seen to the South as a purple/mauve and white band. In the rectangular

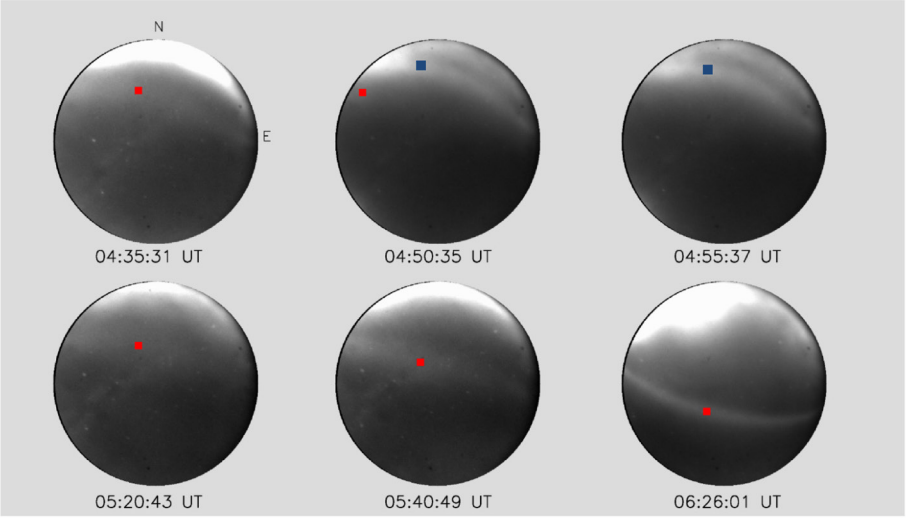

Figure 2. 630.0 nm Images from Bridger all-sky imager using zenith angles less than 80°. Aurora and a weak SAR arc (indicated by a *red square*) are observed all night. A brighter strong thermal emission velocity enhancement (shown by a *blue square*) appears at 04:50 and 04:55 UT. At 05:20 UT the weak SAR arc becomes more visible and it is the only subauroral structure seen the rest of the night, becoming brighter after ~6:00 UT.

projection STEVE is observed to the left, stretching east-west to the South of the observer, with the main auroral oval in the right.

2.2. All-Sky Imagers

All-sky imagers are optical instruments that measure nighttime airglow emissions at different wavelengths. Widely used for upper atmosphere observations, emissions in 630.0 nm provide information on thermosphere–ionosphere processes occurring from equatorial to high latitudes (Martinis et al., 2018). This emission is the result of the de-excitation of atomic oxygen in the (^{1}D) state. A process typically observed at subauroral latitudes during geomagnetic storms is an east-west elongated arc, brighter than the background airglow, named SAR arc (Barbier, 1960; Kozyra et al., 1997; Mendillo et al., 2013). Visible only in 630.0 nm, SAR arcs share some characteristics with STEVEs, but they are inherently different processes, driven by different mechanisms (Harding et al., 2020).

In the same region of the auroral and STEVE displays observed by the citizen scientist and described in the previous section an all-sky imager was operating at Bridger, Montana (45.3°N, 108.9°W), part of the Midlatitude All-sky-imaging Network for Geophysical Observations (MANGO) network. It measured aurora and a SAR arc all night. This system operates only in 630.0 nm, each image has an integration time of 4 min, and, due to the lack of background filter, absolute calibration cannot be performed. The bright STEVE (~1,000 DN) was observed between 04:50 and 5:05 UT while the weak SAR arc (~300 DN) was observed from 02:50 to 09:30 UT.

Figure 2 shows raw images from Bridger between 04:35 and 06:26 UT. The red squares on the images show the SAR arc and the blue squares at 04:50 and 04:55 UT show the STEVE, much brighter than the SAR arc. After ~06:00 UT the SAR arc brightness intensifies.

2.3. Combining the Two Sets of Optical Data

The location of the two observing systems allows us to determine the height of STEVE using triangulation, as done in Archer, Gallardo-Lacourt, et al. (2019). Images need first to be unwarped, that is assign to each pixel latitude and longitude positions. Raw data capture emission patterns as a function of elevation angle and azimuth. The standard procedure implies obtaining a "distortion function" that relates zenith distance in pixels with zenith distance in degrees. This is done by recording the elevation and azimuth of stars and

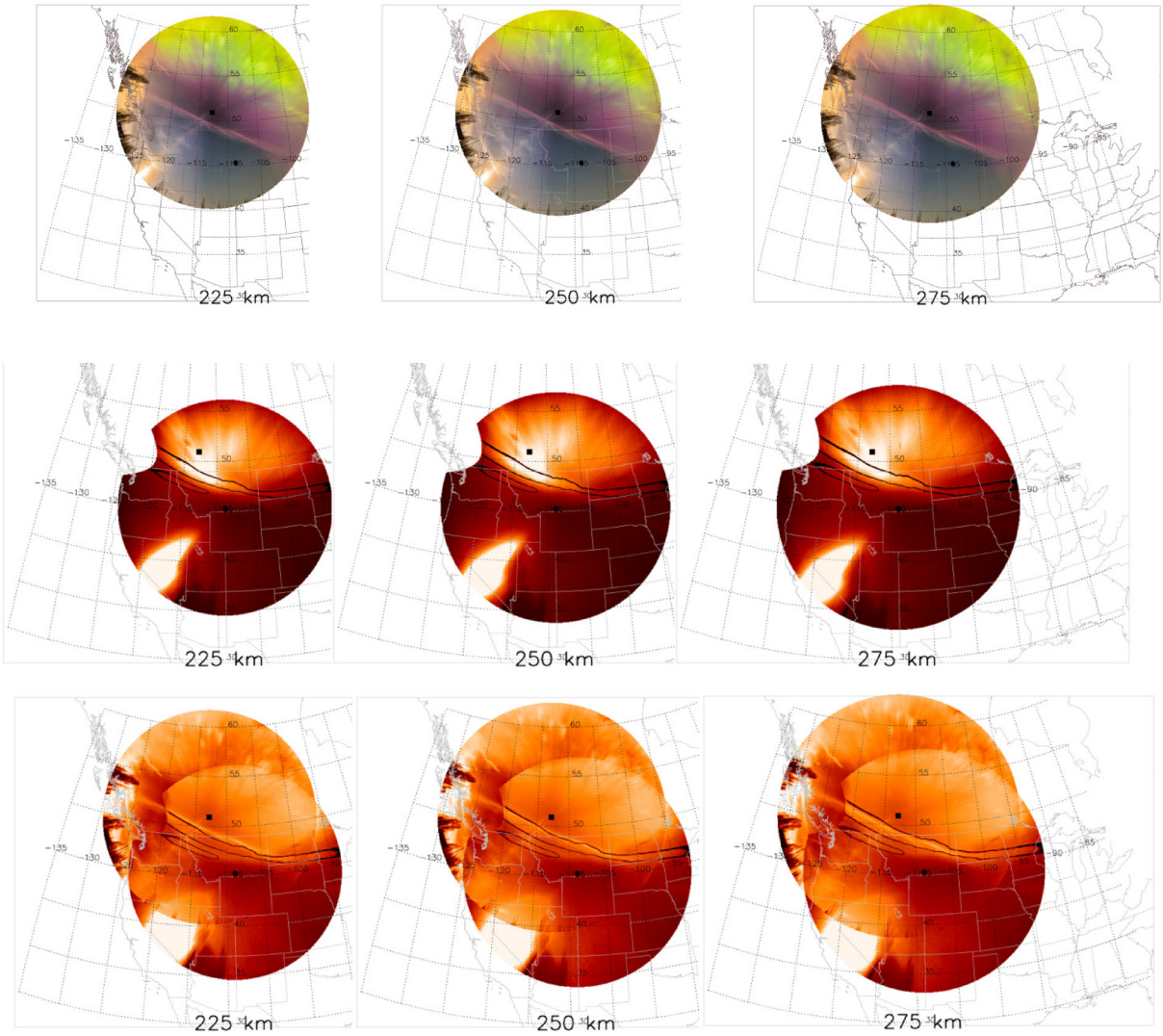

Figure 3. (Top): Unwarped citizen scientist photograph at three different heights (225, 250, and 275 km) using zenith angles less than 80°; (middle): all-sky image from Bridger unwarped at the same heights. The bite out at the top left corner is part if the image not sampled by the CCD chip. Lines representing the width of strong thermal emission velocity enhancement (STEVE) were overlaid. A portion of the weak SAR arc is clearly visible to the left of the image between; and (bottom): merged images at the three heights, using the red channel of the auroral photograph. STEVE is seen to overlap at all longitudes at 250 and 275 km.

their pixel locations in the image. Once an appropriate emission height is chosen, an unwarped version of the raw image is made where each pixel has a unique geographic latitude and longitude. The range of altitudes chosen to process the images went from 200 to 400 km. The largest latitudinal offsets in the location of STEVE were for the low and high unwarping altitudes. Here, we show the results obtained for 225, 250, and 275 km. The top panel in Figure 3 shows the unwarped all-sky image from Alberta at these heights using zenith angles less than 80°. STEVE occurs to the South of the photographer's location (black square) and North of Bridger's zenith (black circle). The middle panel shows the unwarped images from Bridger ASI using the same heights and zenith angle as the top panel. To facilitate the comparison, the edges of the bright STEVE and weak SAR arc are traced with black lines. The locations of the photographer (open black square) and Bridger's zenith (filled black circle) are shown. The STEVE is observed to the North of the ASI's zenith. The bright light to the South is the Moon. The bottom panel shows the superposition of the two images. Only the red channel images from the top panel are overlaid with the corresponding images from the middle panel. At 250 and 275 km the two systems observe STEVE at the same location. The match between the structures is not so good at 225 (and even worse at 200 km and altitudes higher than 300 km,

not shown). There are morphological differences, for example, the 630.0 nm STEVE is brighter in the West and its eastern edge becomes more zonally aligned, almost merging with the existing weak SAR arc. The Alberta STEVE looks very uniform along the entire arc and it does not show any tilt in its eastern edge. These differences could point to different excitation mechanisms between the STEVE and the red SAR arc.

2.4. Satellite Data

Several Swarm and DMSP satellite passes over North America are available during this night, but between ~04:00 and ~05:00 UT, there are no passes within the fields of view of the ground-based observations. At ~04:08 UT, DMSPF18 was at the magnetically conjugate location of the Bridger ASI moving at ~865 km. The trajectory of the satellite is mapped into the northern hemisphere using IGRF-13 (Thébault et al., 2015) and defining quasi-dipole coordinates (Richmond, 1995). Figure 4A shows the DMSPF18 trajectory mapped into the Bridger all-sky image at 300 km (left).The black circle represents Bridger's zenith. The overlaid red line indicates the width of the SAR arc. The plasma density (N_e) shows a broad region with decreased values coinciding with the SAR arc location. The horizontal ion velocity shows a peak of ~2 km/s slightly offset from the decreased N_e. These two parameters are measuring SAPS-like conditions that are typically associated with SAR arcs (Foster et al., 1994). If the trajectory were mapped to 350 km then the location of the SAR arc would be closer to the peak in ion velocity and not fully in the region of significant decrease in N_e. The electron temperature (T_e) was not available. At ~04:29 UT Swarm-C, moving at 530 km, crossed the magnetically conjugate region and the T_e and N_e signatures were consistent with the ones typically observed during SAR arc events, that is, a wide T_e enhancement and N_e reduction, reaching a minimum of $\sim 1 \times 10^4$ el/cm^3. This is shown in Figure 4B. In addition, deeper and narrower N_e decrease (reaching $\sim 2 \times 10^3$ el/cm^3) and T_e enhancement are observed. They occur poleward from the SAR arc and do not have a corresponding optical signature. At ~04:50 UT, DMSPF17 crossed the same region sampled earlier by Swarm-C in the southern hemisphere. Its trajectory was mapped into the northern hemisphere and plotted on top of the Bridger image taken at 04:50 UT. Figure 4C shows the zoomed in Bridger image, unwarped at 300 km, with the trajectory of DMSPF17 (white line). The thin blue line indicates the width of the STEVE and the red line the width of the weak SAR arc. To the right, from top to bottom, N_e, T_e, and horizontal ion velocity are plotted. The inset blue and red lines in each panel represent the location of the mapped DMSP trajectory along the STEVE and SAR arc, respectively, at different unwarped heights (from 200 to 375 km). A sharp T_e enhancement that reaches ~6,000 K and a minimum in N_e are observed at ~48°Glat. A broader T_e enhancement and reduced N_e are also observed equatorward. A very large westward flow of ~5 km/s is also measured at the location of the sharp T_e enhancement, clear evidence of intense SAID, usually associated with STEVE. The best matches between the location of STEVE and SAR arc and the plasma data from DMSP occur between 200 and 250 km for STEVE, and between 300 and 350 km for SAR arc. No indication of large westward flow related to the SAR arc is observed. This points to inherent differences in generation mechanisms to excite airglow emissions in the two optical processes (in situ ion-drag for STEVE, and heat transfer from the inner magnetosphere for SAR arc).

3. Discussion and Summary

On September 28, 2017 aurora and subauroral optical phenomena were observed from the ground. The subauroral processes consisted of a long-lived SAR arc observed in 630.0 nm and a short-lived multiwavelength STEVE. DMSP and Swarm satellites provided plasma data related to the optical phenomena. This study combines for the first-time citizen scientist photographs and all-sky images, as well as conjunctions with satellite data, of STEVE.

The Alberta all-sky image constructed from individual frames was compared with the all-sky image from Bridger. After obtaining the distortion functions of the all-sky images they were compared assuming different emission heights. While each image from Alberta had an exposure time of 10 s, the exposure time of the Bridger image was 4 min. Thus, the fine structuring (consisting at some places of 2–3 thin separated arcs) observed with the Alberta camera is wiped out in the long exposure image from Bridger that shows a relatively wide single arc. The fine structuring could also be involving emissions not sampled by the Bridger ASI. The equatorward motion of STEVE could also have an effect on the determination of the height of emission due to the long integration time of the Bridger image. While the overlaid images at 250 and

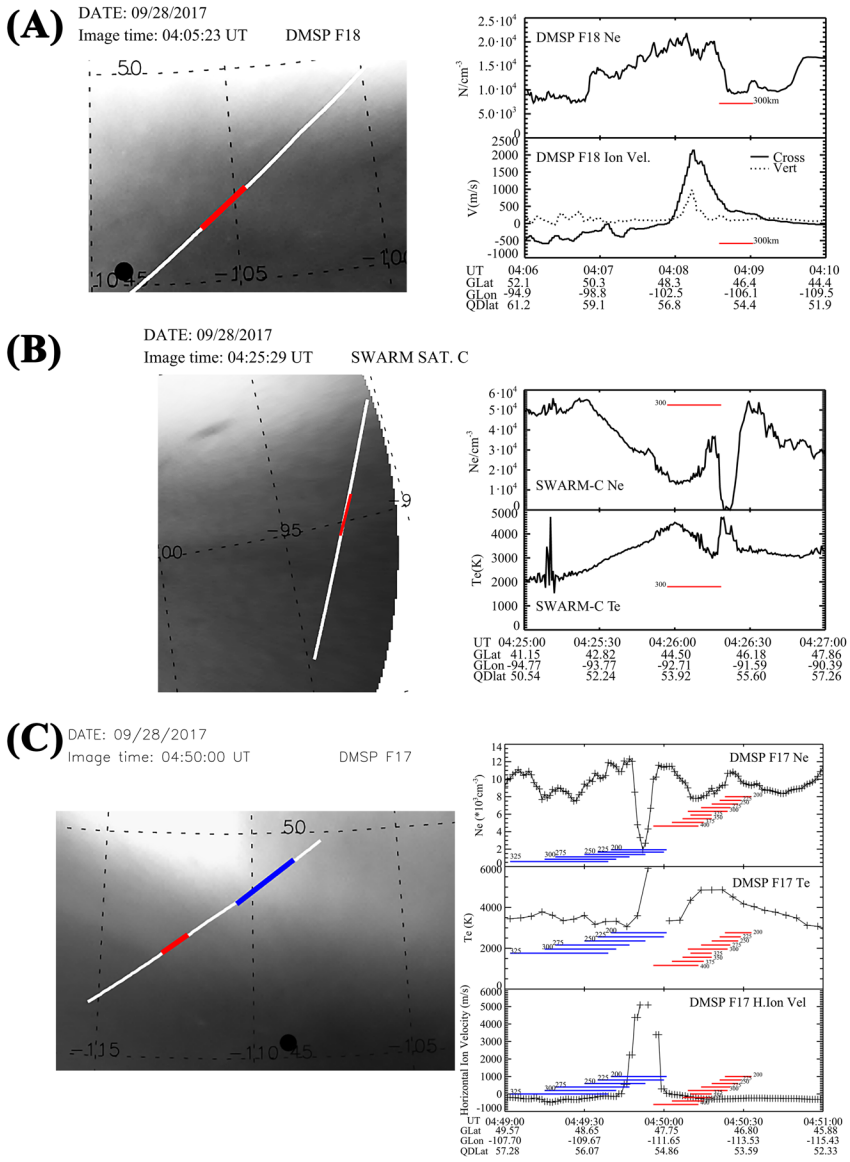

Figure 4. (Left): Satellite trajectories mapped from the southern hemisphere into the Bridger all-sky image (*white* line) at 300 km. The overlaid *red* lines mark the locations of the SAR arc; (right): Plasma parameters measured by the satellites. (**A**) DMSPF18 at ~04:08 UT. Plasma density N_e shows a small decrease coinciding with the SAR arc location. The horizontal ion velocity shows a peak of ~2 km/s slightly offset from the decreased N_e. No electron temperature was available; (**B**) Swarm C satellite at ~04:26 UT. The plasma data show a wide density trough and a wide enhanced electron temperature. The *red* lines indicate where the SAR arc is observed. Deeper and narrower N_e decrease and T_e enhancement are observed poleward from the SAR arc. There is no corresponding optical signature, but these might be precursor conditions leading to the strong thermal emission velocity enhancement (STEVE) observed later (see text); (**C**) DMSPF17 at ~04:50 UT. The *red* and *blue* lines show the location of the SAR arc and STEVE, respectively, when the image is unwarped at different altitudes. The sharp and large changes in the three plasma values at ~48°Glat coincide with the STEVE location in the 200–250 km range. The broader and smaller changes at lower latitude coincide with the SAR arc location in the 300–350 km range.

275 km in Figure 3 show a better match, the proper height range could be between 225 and 250 km. This height range is in agreement with the heights obtained in Archer, Gallardo-Lacourt et al. (2019) and Liang et al. (2019). Harding et al., (2020) proposed a mechanism to explain the source of emission of STEVE that works when the peak airglow occurs around 130 km, being almost zero above 220 km. Our results showing a height of emission near 225–275 km imply that the mechanism proposed in Harding et al. (2020) and Liang et al. (2019) needs to be revisited to incorporate enhanced 630.0 nm airglow at these heights. A

possible mechanism was proposed by Sazykin et al. (2002) when trying to explain a weak 630.0 nm SAR arc that involved ion-drag heating and excitation of neutral species due to large westward plasma flows. This could be happening in our case, with westward flows close to ~5 km/s.

In general, weak 630.0 nm enhancement is expected in STEVE. But here we have shown that the Bridger ASI measures very bright STEVE in 630.0 nm, similar to the auroral intensity. It also shows stronger emissions in its western part, while the colocated Alberta multiwavelength STEVE seems to be very uniform in brightness. The latitudinal separation between STEVE and SAR arc, as observed by Bridger, seems to be very small in the eastern part of the image, as if the two structures were merging.

In situ plasma data related to STEVE and SAR arc were obtained from satellite measurements. While no satellite data were available at the time of the STEVE observation in the northern hemisphere, geomagnetic conjugate measurements between ~4:05 and ~4:50 UT were used. At ~04:08 UT, DMSPF18 was crossing the magnetically conjugate location of Bridger ASI and detected strong westward flows of about 2 km/s and a wide decrease in plasma density. Mapping the trajectory into the northern hemisphere, these perturbations in the plasma parameters coincide with the location of the SAR arc observed at Bridger under reasonable uncertainty of the actual emission height. This is compatible with the existing notion of the connection between SAPS and SAR arcs. The lack of a large decrease in plasma density at the time of the velocity peak could be due to the fact that the topside density might not have had enough time to respond to large density decreases in the F-region peak, as shown in Anderson et al. (1991). Later at ~04:26 UT, at a lower altitude and ~10° to the East of the DMSPF18 pass, Swarm-C also showed typical signatures associated with SAR arcs, that is, T_e enhancement and N_e decrease, that when mapped into the northern hemisphere coincided with the SAR arc. Interestingly, additional plasma perturbations in T_e and N_e are observed ~1–2° poleward, and when mapped into the northern hemisphere, they are related to a structure-less and uniform background airglow over Bridger. The changes are sharper than the ones associated with the observed SAR arc and look similar to the sharp signatures that will be observed later by DMSPF17. It is not clear why airglow perturbations are not occurring, but it is something to take into account because similar plasma perturbations are detected when STEVE is observed later. T_e is already elevated but its magnitude does not always correlate with SAID. Not only high T_e but also strong SAID seems to be necessary conditions for STEVE to occur (Nishimura et al., 2020). The plasma density also decreased significantly. Most likely SAID was developing at that time and a substorm occurring later may have strengthened SAID and the energy input became large enough to produce STEVE. Figure S1 shows Supermag indices AU (SMU) and AL (SML) (Gjerloev, 2012) between 04:00 and 09:00 UT. Several substorms are observed during this period. The first one has the main phase ending at ~04:30 UT, with a recovery phase lasting until ~05:00 UT. It is during the recovery phase of this substorm that STEVE is observed, in agreement with studies showing that STEVE is a substorm recovery phase phenomenon (Gallardo-Lacourt, Nishimura, et al., 2018). The other substorms seem to contribute to the energization of the SAR arc that becomes brighter after ~06:00 UT and moves equatorward until ~10:00 UT.

The satellite data directly related to STEVE come from DMSPF17. At ~04:50 UT it was moving in the southern hemisphere at 875 km in a trajectory that when mapped into the northern hemisphere coincided with the optical signatures associated with STEVE and SAR arc. Figure 4B shows a zoomed in Bridger image unwarped at 300 km with lines indicating the location of STEVE and SAR arc, and plasma parameters measured by DMSPF17. Two noticeable features are observed: first, a sharp T_e enhancement that reaches ~6,000 K and a collocated minimum in N_e, and, second, a broader T_e enhancement and reduced N_e occurring equatorward. A very large westward flow of ~5 km/s is also measured at the location of the sharp T_e enhancement, clear evidence of intense SAID conditions. No indication of large westward flow related to the SAR arc is observed, providing evidence of an inherent difference in the generation mechanism that seems to favor ion-drag heating for STEVE, and heat conduction, or particle precipitation of soft electrons, for SAR arc. We can assume that the initial perturbations detected by Swarm-C at ~4:26 UT (Figure 4B) are related to the perturbations measured by DMSPF18 at ~4:50 UT (Figure 4C). It is not clear how long plasma perturbations and what particular conditions are needed to produce STEVE. While it is observed initially at ~4:50 UT, large plasma perturbations were present at ~4:26 UT meaning that perhaps the conditions to generate STEVE started to evolve at least 30 min before the optical detection. STEVE formation

mechanisms are not fully understood, and the sequence of observations described here might provide clues to understand how STEVE is generated.

The range of heights where the plasma perturbations better match the optical signatures associated with STEVE and SAR arc can be investigated by mapping the trajectory of the satellite into the image unwarped at different heights. Both optical processes occur at different heights. The altitude range for STEVE is between 200 and 250 km, and for SAR arc between 300 and 350 km. Thus, from the DMSP analysis shown in Figure 4C and the results from Figure 3 we can estimate that the STEVE is occurring between 200 and 250 km at 04:50 UT and between 225 and 275 km at 04:55 UT (if no adjustment is made to take into account the evolution of STEVE).

To summarize, for the first time Citizen Scientist data and scientific data from an all-sky imager are combined to show the simultaneous occurrence of a STEVE on September 28, 2017. Both data sets also measured aurora, but only the scientific camera was able to detect a weak SAR arc occurring all the night. At 04:50 UT, DMSPF17 was moving through the magnetically conjugate location of Bridger ASI. When the trajectory is mapped into the northern hemisphere the satellite data detected plasma signatures related to STEVE and SAR arc. A large westward flow of ∼5 km/s was observed only at the STEVE location. From these two sets of comparisons, that is, two optical systems and satellite and ASI, the height of STEVE was determined to be between 200 and 250 km at 04:50 UT and between 225 and 275 km at 04:55 UT. STEVE's brightness was not uniform in the 630.0 nm images and it appeared as a wide structure, while the white light image from Alberta shows a relatively uniform bright arc, formed by 2–3 thin individual spread out arcs. STEVE was observed during the recovery phase of a weak substorm. We have shown hints of STEVE formation process by detecting initial plasma perturbations in N_e and T_e from Swarm-C before the occurrence of STEVE. These perturbations are similar in intensity and shape to the ones observed by DMSPF17 when STEVE is occurring, prompting to speculation that a "build up" is necessary before the environment responds optically to the plasma perturbations.

Data Availability Statement

DMSPF17 and F18 data were obtained from the CEDAR Madrigal website http://cedar.openmadrigal.org/static/experiments3/2017/dms/28sep17/ as daily ASCI files from the SSIES instrument. The all-sky citizen scientist image is available at https://doi.org/10.5281/zenodo.4557666. Raw Bridger images used in this study are available at https://doi.org/10.5281/zenodo.4557677. Swarm data were obtained from https://swarm-diss.eo.esa.int/#swarm%2FLevel1b%2FLatest_baselines%2FEFIx_LP as daily CDF files for the EFI instrument. SuperMAG data were obtained from http://supermag.jhuapl.edu/indices/?layers=SME.UL&fidelity=low&start=2017-09-28T04%3A00%3A00.000Z&step=4320&tab=plot.

Acknowledgments
C. Martinis was supported by NASA HGI Grant 80NSSC19K0546 and by NSF Aeronomy AGS-1552301. Y. Nishimura work was supported by NSF Aeronomy grant AGS-1907698, by NASA HGI Grant 80NSSC18K0657, and by AFOSR Grant FA9559-16-1-0364. The MANGO camera installation at Bridger was supported by NSF AGS grant # 1452357. B. Gallardo-Lacourt was supported by a NASA Postdoctoral Program Fellowship.

References

Anderson, P. C., Heelis, R. A., & Hanson, W. B. (1991). The ionospheric signatures of rapid subauroral ion drifts. *Journal Geophysical Research*, *96*(A4), 5785–5792. https://doi.org/10.1029/90JA02651

Archer, W. E., Gallardo-Lacourt, B., Perry, G. W., St. Maurice, J. P., Buchert, S. C., & Donovan, E. (2019). Steve: The optical signature of intense subauroral ion drifts. *Geophysical Research Letters*, *46*, 6279–6286. https://doi.org/10.1029/2019gl082687

Archer, W. E., St.-Maurice, J., Gallardo-Lacourt, B., Perry, G. W., Cully, C. M., Donovan, E., et al. (2019). The vertical distribution of the optical emissions of a STEVE and picket fence event. *Geophysical Research Letters*, *46*, 10719–10725. https://doi.org/10.1029/2019gl084473

Barbier, D. (1960). L'arcauroral stable. *Annales Geophysicae*, *16*, 544–549.

Foster, J. C., Buonsanto, M. J., Mendillo, M., Nottingham, D., Rich, F. J., & Denig, W. (1994). Coordinated stable auroral red arc observations: Relationship to plasma convection. *Journal of Geophysical Research*, *99*(A6), 11429–11439. https://doi.org/10.1029/93JA03140

Gallardo-Lacourt, B., Liang, J., Nishimura, Y., & Donovan, E. (2018). On the origin of STEVE: Particle precipitation or ionospheric skyglow? *Geophysical Research Letters*, *45*, 7968–7973. https://doi.org/10.1029/2018GL078509

Gallardo-Lacourt, B., Nishimura, Y., Donovan, E., Gillies, D. M., Perry, G. W., Archer, W. E., et al. (2018). A statistical analysis of STEVE. *Journal of Geophysical Research: Space Physics*, *123*, 9893–9905. https://doi.org/10.1029/2018JA025368

Gillies, D. M., Donovan, E., Hampton, D., Liang, J., Connors, M., Nishimura, Y., et al. (2019). First observations from the TREx spectrograph: The optical spectrum of STEVE and the picket fence phenomena. *Geophysical Research Letters*, *46*, 7207–7213. https://doi.org/10.1029/2019gl083272

Gjerloev, J. W. (2012). The SuperMAG data processing technique. *Journal of Geophysical Research*, *117*, A09213. https://doi.org/10.1029/2012JA017683

Harding, B. J., Mende, S. B., Triplett, C. C., & Wu, Y. J. J. (2020). A mechanism for the STEVE continuum emission. *Geophysical Research Letters*, *47*, e2020GL087102. https://doi.org/10.1029/2020gl087102

Kozyra, J. U., Nagy, A. F., & Slater, D. W. (1997). High-altitude energy source(s) for stable auroral red arcs. *Reviews of Geophysics*, *35*, 155–190. https://doi.org/10.1029/96rg03194

Liang, J., Donovan, E., Connors, M., Gillies, D., St. Maurice, J. P., Jackel, B., et al. (2019). Optical spectra and emission altitudes of double-layer STEVE: A case study. *Geophysical Research Letters*, *46*, 13630–13639. https://doi.org/10.1029/2019gl085639

MacDonald, E. A., Donovan, E., Nishimura, Y., Case, N. A., Gillies, D. M., Gallardo-lacourt, B., et al. (2018). New science in plain sight: Citizen scientists lead to the discovery of optical structure in the upper atmosphere. *Science Advances*, *4*, 16–21. https://doi.org/10.1126/sciadv.aaq0030

Martinis, C., Baumgardner, J., Wroten, J., & Mendillo, M. (2018). All-sky-imaging capabilities for ionospheric space weather research using geomagnetic conjugate point observing sites. *Advances Space Research*, *61*(7), 1636–1651.

Mendillo, M., Baumgardner, J., Wroten, J., Martinis, C., Smith, S., Merenda, K. D., et al. (2013). Imaging magnetospheric boundaries at ionospheric heights. *Journal of Geophysical Research: Space Physics*, *118*, 7294–7305. https://doi.org/10.1002/2013JA019267

Nishimura, Y., Donovan, E. F., Angelopoulos, V., & Nishitani, N. (2020). Dynamics of auroral precipitation boundaries associated with STEVE and SAID. *Journal of Geophysical Research: Space Physics*, *125*, e2020JA028067. https://doi.org/10.1029/2020ja028067

Nishimura, Y., Gallardo-Lacourt, B., Zou, Y., Mishin, E., Knudsen, D. J., Donovan, E. F., et al. (2019). Magnetospheric signatures of STEVE: Implications for the magnetospheric energy source and interhemispheric conjugacy. *Geophysical Research Letters*, *46*, 5637–5644. https://doi.org/10.1029/2019gl082460

Richmond, A. D. (1995). Ionospheric electrodynamics using magnetic apex coordinates. *Journal of Geomagnetism and Geoelectricity*, *47*, 191–212. https://doi.org/10.5636/jgg.47.191

Sazykin, S., Fejer, B. G., Galperin, Y. I., Zinin, L. V., Grigoriev, S. A., & Mendillo, M. (2002). Polarization jet events and excitation of weak SAR arcs. *Geophysical Research Letters*, *29*(12). https://doi.org/10.1029/2001GL014388

Thébault, E., Finlay, C. C., Beggan, C. D., Alken, P., Aubert, J., Barrois, O., et al. (2015). International geomagnetic reference field: The 12th generation. *Earth, Planets and Space*, *67*(1), 79. https://doi.org/10.1186/s40623-015-0313-0